

DIGITAL CAMERAS AND THEIR APPLICATION TO DIGITAL PHOTOGRAMMETRY FOR LANDFORM MODELING

Mladen Stojic¹ and Julie Shannon²

¹ Digital Photogrammetric Engineer, ERDAS Inc., International Division
2801 Buford Hwy, N.E., Suite 300, Atlanta, Georgia 30329-2137 USA

² Ph.D. Candidate, Department of Geography, King's College, London, Strand
London, WC2R 2LS, United Kingdom

ISPRS Commission II, Working Group 7
Practical and Implementation Issues in Digital Mapping

KEYWORDS: digital cameras, camera calibration, self-calibration, digital elevation model, geomorphology, landform modeling

ABSTRACT

The utilization of digital cameras for applications associated with close-range photogrammetry have also been extended to their use with aerial photogrammetric applications. This paper reviews the application of digital photogrammetry to landform modeling using a digital camera. Using a Kodak DCS420 digital camera, a strip of 1:45,000 scale imagery was collected. The ERDAS IMAGINE OrthoBASE™ digital photogrammetry software package was used to perform the self-calibrating bundle adjustment (SCBA). The geometric information describing the digital cameras internal geometry was determined. This includes the focal length, principal point offset in the x and y direction and additional parameters accounting for radial lens distortion, non-orthogonality of the x and y image axis and scale differential factor for the variation in x and y pixel size. The paper defines a suitable approach for simultaneously recovering the interior and exterior orientation parameters of the camera using statistical properties of the input observations and unknown parameters. The quality of the SCBA was verified by automatically generating digital elevation models (DEM) and comparing the results with field survey check points. Using the strip of 1:45,000 imagery, elevation accuracies were approximately 0.5 meters.

1. INTRODUCTION

Recent advances in digital camera technology and image processing have allowed for the smooth integration between image acquisition and data extraction using digital photogrammetry. Such integration has enabled new applications to be realized within the subject fields of topographic mapping, landform modeling, infrastructure management, geomorphology, medical, architectural and industrial photogrammetry. The flexibility inherent with a purely digital solution allows terrestrial, close range, and aerial photogrammetric applications to be realized using the same digital data acquisition device.

Most of the currently available off-the-shelf digital cameras may be considered non-metric, where parameters used to model the camera's internal geometry are unknown. Due to the high geometric accuracies required, the geometric information describing the digital cameras internal geometry must be determined. The photogrammetric procedure used to estimate the internal geometry is referred to as self-calibration and determines the best estimates for Additional Parameters (APs) used to define the camera's internal geometry as existed during image exposure. This includes focal length of the camera, principal point offset, lens distortion, differential image axis scaling and non-orthogonality between the x and y image axis scale. Studies indicate that analytical self-calibration techniques can be utilized successfully in accurately recovering both the interior and exterior orientation parameters (Kenefick *et al.*, 1972; Fraser, 1997). Although previous studies have focused on self-calibration for close-range photogrammetric

applications, this research study attempts to extend the use of self-calibration for digital photogrammetric applications involved with landform modeling.

This paper focuses on the effective use of digital cameras for applications involved with aerial mapping using softcopy photogrammetry, particularly those associated with landform modeling for geomorphological applications.

This paper aims at defining the issues associated with using commercially available digital cameras for digital photogrammetric operations, particularly related to the use of self-calibration techniques for simultaneously recovering interior and exterior orientation parameters. Important issues include: the impact of using varying interior orientation models within existing photogrammetric functional models; assessing accuracies attainable and examining correlations between interior and exterior orientation parameters.

2. BACKGROUND

Photogrammetry has been used as a source of landform information in a variety of geomorphic applications (Welch and Jordan, 1983; Collin and Chisholm, 1991) but the advent of analytical and, more recently, digital photogrammetry has opened new applications for photogrammetry in the acquisition of geomorphic data (Lane *et al.*, 1993; Fryer *et al.*, 1994; Chandler and Brunsden, 1995; Dixon *et al.*, 1996). Digital photogrammetric applications have also been extended to the use of non-metric cameras for the collection of photography

(Stojic *et al.*, 1998), where a self-calibrating bundle adjustment (SCBA) was used to recover the parameters associated with interior orientation.

A digital elevation model (DEM) can be considered as a representation of the continuous surface of the ground by a large number of selected XYZ coordinates (Chandler and Moore, 1989). The three-dimensional representation offered by a high resolution DEM, is one of the more advantageous models which can be used to represent three-dimensional characteristics of a landform.

3. GEOMORPHOLOGICAL PROBLEM

Ephemeral channels are characterized by irregular and complex channel bed morphology. In this study the channel bed form is one of the key elements, particularly the braided channel systems that incise the gravel bed. It is this braided system that

determines the flow characteristics, amount of water and sediment transported or deposited. Accurate representations of such landforms are required for the derivation of information needed to model flow and sediment transport characteristics.

During field data collection it is normally feasible to survey cross-sectional grids down a channel. As Lane *et al* (1994) point out, cross-section profiles provide indicators concerning cross-stream profiles and processes, but little about the linkages and processes downstream. Thus downstream profiles are equally important and required. Using a DEM, a large number of closely spaced cross-sectional profiles downstream can be extracted in order to provide information about the downstream profile. This information can then be used in hydrologic models of water and sediment transport in ephemeral channels that are currently being developed.

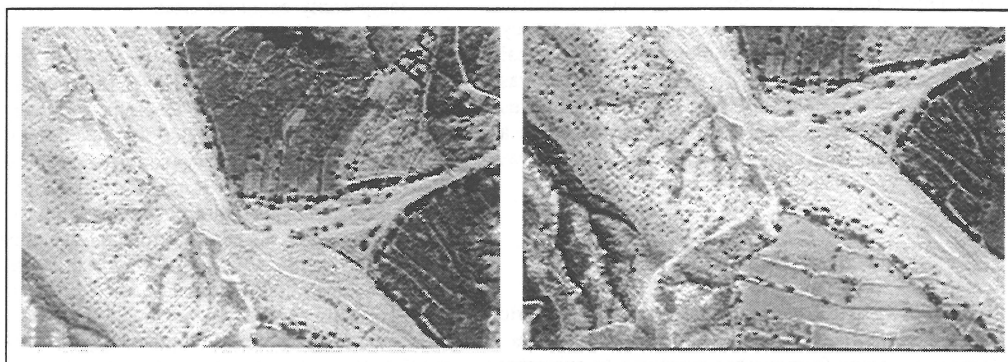


Figure 1. 1:45,000 Overlapping images obtained using the Kodak DCS420 digital camera

4. STUDY SITE

The Nogalte catchment is a sub-catchment of the Río Guadalentín in the provinces of Murcia and Almería, located in southeast Spain. The area is classified as semi-arid, experiencing highly variable rainfall, with averages between 300-350 mm per year. The channel is 33 km in length serving a catchment of 171km². The area is predominantly mica schist, with approximately half of the catchment given over to agriculture; predominantly almonds, olives and some wheat cultivation on the flood terraces in the main channel. The other land covers include matorral on hillslopes unsuitable for cultivation, and riparian vegetation on the channel bed. The study site is a tributary junction, where the Rambla Cárdena joins the main channel. The channel bed is gravel, with an incised fan at the channel junction. The area of the DEM covers both up and downstream portions of the Cárdena junction.

5. DATA ACQUISITION

Digital imagery of the Rambla Nogalte was obtained April 1997 using two KODAK DCS420 digital cameras, one panchromatic and one color infrared (CIR). The cameras were configured for use with the Aerial Digital Photographic System (ADPS). The ADPS comprises a Nikon N90 camera, with a focal length of 28 mm, but the film emulsion is replaced with a charge-coupled device (CCD) array. The CCD sensor digitally records 1525 pixels horizontally and 1012 pixels vertically. The physical imaging dimensions of the CCD are 14 mm by 9.3 mm in the horizontal and vertical direction, respectively. This

amounts to a pixel size of approximately 9.2 microns. Although a variation of 0.009 microns exists between the pixel size in the x and y direction. Due to the digital nature of the camera, fiducial marks were not available. The only internal reference points suitable for defining a reference system in the image space were the corners of image format (Smith, 1987; Stojic *et al.*, 1998).

A twin engined Partanavia P28 aircraft with a photographic port was used to capture a photogrammetric strip of 3 images (Figure 1). The average flying height was 1246 meters above ground level, where the ground level ranged between approximately 600 to 620 meters above sea level. This produced image pixels that covered an area of 0.16m² or 0.40 meters, ground coverage per pixel. The average photo scale is 1:45,000. Each pair of images had 60 percent overlap. The black and white images occupied approximately 1.5Mb each.

5.1 Survey Data

Five reference survey stations were defined prior to establishing the ground control points (GCPs). The stations were approximately 180 meters separated. Differential GPS data was collected using a Wild GPS System 200 with a SR399 antenna and CR333 controller. Using the accompanying SKI 2.2 software, the exact locations of the five survey stations within the Universal Transverse Mercator (UTM) Projection, Zone 30S and WGS 84 reference datum were determined. The X, Y, Z positions of all surveyed GCPs and check points were transformed onto this projection.

Using a SOKKIA Set 4B Total Station, 56 GCPs were surveyed from five reference survey stations. In areas where the channel bed was dry, black plastic sheeting was chosen for the setting of ground control markers. The plastic sheeting was cut into 0.64m² squares, where each sheet covered an area of 4 pixels. The center of each sheet was surveyed. Due to the nature of the terrain and land cover, many areas were inaccessible for the placement and measurement of GCPs. The majority of points were evenly and spatially distributed within the channel beds and floodplain. The GCPs were collected to a precision of 0.10 meters in X and Y and 0.20 meters in the Z direction.

Known X, Y, Z survey points, other than those collected as GCPs were required for the validation of automatically generated DEMs. Two visits to the field were made in order to collect 97 validation points, in June and September 1996. A triangulation of three survey stations was established. From the three survey stations, survey points above and below the channel junction were measured, using a SOKKIA Set 4B Total Station. These points were initially transposed onto a Cartesian grid, with the reference point being the first survey reference station. Using the UTM coordinates of the original five reference survey stations, the validation data was transposed onto the UTM Zone 30S map projection. This enabled the GCPs and validation check points to be within a uniform map projection. The validation check point data was collected to an overall precision of 0.17 meters.

6. METHODOLOGY

Using the IMAGINE OrthoBASE digital photogrammetric software package, photogrammetric restitution was carried out. The four corners of image format were measured to sub-pixel accuracy in order to define the image space coordinate system for each frame. Resulting root mean square (RMS) errors were approximately 0.4 μ m. Surveyed GCPs were imported and subsequently measured on the three frames of imagery. Frame two contained 13 GCPs, frame three contained 16 GCPs and frame four contained 9 GCPs. Approximately 21 tie points were measured and spatially distributed among the images, within areas containing no GCP data.

The self-calibrating bundle adjustment capabilities of IMAGINE OrthoBASE were used to simultaneously recover the interior orientation parameters and estimate the exterior orientation parameters of the camera as existed at the time of image exposure. Prior to executing the self-calibration, initial approximations to the unknown exterior orientation parameters were estimated by the software, requiring no a-priori estimates of the camera positions and rotation angles. The numerical models used were advantageous in these circumstances. The self-calibrating bundle adjustment results were optimized by modifying the stochastic model (i.e. input standard deviation's) representing the precisional quality of the input observations (i.e. image measurements, GCP data) and unknown interior and exterior orientation parameters. The overall aim was to decrease the global standard error of the solution, standard deviations of the individual exposure stations and accuracy of the GCPs. The software provided these values. It was also important to ensure that the recovered interior orientation parameters had standard errors substantially smaller than the parameters themselves. Additional parameters (AP) were introduced into the solution once a geometrically stable photogrammetric configuration had been established with respect to initial approximations to the exterior orientation. This included the definition of an appropriate stochastic model

for the image measurements, GCPs and exterior orientation parameters.

The estimated interior and exterior orientation parameters were subsequently used within IMAGINE OrthoMAXTM in order to automatically generate stereo-pairs and DEMs. The validation data was then used to assess the quality of the DEM thus inferring the accuracy of the self-calibrating bundle adjustment.

7. RESULTS AND DISCUSSION

The results from performing the self-calibrating bundle adjustment are shown in Table 1. Prior to executing the self-calibration initial approximations to the unknown exterior orientation parameters (X, Y, Z, omega, phi, kappa) for all three frames comprising the strip were estimated. A fixed focal length (f = 28.0 mm) was assumed and zero assignments to the principal point offset in the x and y direction were used (*Run 1*). Due to relatively large standard deviation values, frame 4 was temporarily excluded from further processing (*Run 2*). In the subsequent iteration of processing, the interior orientation (f, xp, yp) and exterior orientation parameters were simultaneously estimated (*Run 3*). This yielded a substantially larger standard error (5.4194), along with very large standard deviation results for the exterior orientation parameters. This can be attributed to the over-parameterization of the functional model while using weak initial approximations to the exterior orientation parameters with no corresponding stochastic model. For these reasons, the exterior orientation estimates from Run 2 were used as the new initial approximations (*Run 4*). The interior orientation parameters were excluded from the solution. This resulted in a reduction of the global standard error (0.0063) while strengthening the geometric camera configuration in object space. Based upon the standard deviation values of the newly estimated exterior orientation parameters, statistical weights were assigned to the individual parameters accordingly (*Run 5*). Corresponding output EO standard deviation values were substantially decreased, as were the X, Y and Z accuracy estimates.

Due to the increased stability of the geometric camera configuration, through the use of statistical weights, the interior orientation parameters were estimated (*Run 6*). Compared to Run 3, substantially lower standard errors were achieved for the focal length and principal point offset. In addition to constraining the exterior orientation parameters, statistical weights were assigned to the GCP coordinates (*Run 7*). The introduction of GCP weights to the stochastic model substantially decreased the global standard error and standard deviation results for the exterior orientation parameters. Although weaker accuracies were obtained for the control points and larger standard errors to the estimated interior orientation parameters were generated. By over-constraining the exterior orientation parameters through the use of statistical weights, residual error within the functional model was distributed between the control points and interior orientation parameters. By allowing the GCPs to 'flex' within the limits of their respective standard deviation assignments, residual error was distributed within the observations.

In order to identify and establish the influence of estimating the interior orientation parameters within a geometrically weak photogrammetric network of observations, the interior orientation parameters were temporarily removed from processing (*Run 8*). This resulted in providing a lower global standard error, reduced exterior orientation standard deviation values and increased accuracy in the GCPs. Over-parameterizing the functional model while also using an

| Run | Standard Error (mm) | Exterior Orientation Parameter Std. Dev | | | | | | Accuracy of Control | | | Interior Orientation and Std. Deviations | | | | | |
|-----|---------------------|---|-------|-------|---------------|-------------|---------------|---------------------|-------|-------|--|-----------------|---------|-----------------|---------|-----------------|
| | | X (m) | Y (m) | Z (m) | Omega Dec.deg | Phi Dec.deg | Kappa Dec.deg | X (m) | Y (m) | Z (m) | f (mm) | Std. Error (mm) | xp (mm) | Std. Error (mm) | yp (mm) | Std. Error (mm) |
| 1 | 0.0059 | 6.6 | 7.8 | 1.4 | 0.36 | 0.31 | 0.04 | 0.471 | 0.514 | 3.027 | 28 | | 0 | | 0 | |
| 2 | 0.0063 | 7.5 | 8.8 | 1.6 | 0.41 | 0.34 | 0.05 | 0.576 | 0.644 | 3.715 | 28 | | 0 | | 0 | |
| 3 | 5.4194 | 29.1 | 14.2 | 194.2 | 0.48 | 1.09 | 0.07 | 1.411 | 0.703 | 3.803 | 30.159 | 4.44 | 0.3054 | 0.3847 | 0.7734 | 0.6175 |
| 4 | 0.0063 | 7.5 | 9.0 | 1.7 | 0.41 | 0.35 | 0.05 | 0.576 | 0.644 | 3.715 | 28 | | 0 | | 0 | |
| 5 | 0.0057 | 4.8 | 4.8 | 1.1 | 0.22 | 0.22 | 0.04 | 0.508 | 0.526 | 3.203 | 28 | | 0 | | 0 | |
| 6 | 0.0055 | 6.2 | 6.0 | 6.5 | 0.26 | 0.29 | 0.05 | 0.514 | 0.566 | 3.210 | 28.2465 | 0.148 | 0.1922 | 0.169 | 0.2727 | 0.189 |
| 7 | 0.002 | 3.1 | 2.6 | 2.3 | 0.12 | 0.13 | 0.12 | 2.360 | 4.570 | 1.490 | 28.6472 | 0.9753 | -0.0268 | 0.1026 | 0.0552 | 0.0863 |
| 8 | 0.0018 | 1.9 | 1.8 | 2.1 | 0.08 | 0.09 | 0.11 | 0.377 | 0.356 | 1.356 | 28 | | 0 | | 0 | |
| 9 | 0.0018 | 3.8 | 3.6 | 5.2 | 0.16 | 0.17 | 0.21 | 0.667 | 0.695 | 1.418 | 28 | | 0 | | 0 | |
| 10 | 0.0014 | 1.2 | 1.1 | 1.2 | 0.05 | 0.06 | 0.08 | 0.281 | 0.238 | 1.045 | 28 | | 0 | | 0 | |
| 11 | 0.0015 | 1.7 | 1.5 | 1.3 | 0.09 | 0.10 | 0.09 | 1.460 | 2.790 | 1.140 | 28.6286 | 0.5938 | -0.043 | 0.0664 | 0.238 | 0.0568 |
| 12 | 0.004 | 3.5 | 4.1 | 1.9 | 0.13 | 0.29 | 0.16 | 0.304 | 0.286 | 1.599 | 28.2037 | 0.0445 | 0.0267 | 0.0598 | 0.0272 | 0.0612 |
| 13 | 0.004 | 6.1 | 2.6 | 0.7 | 0.11 | 0.16 | 0.04 | 0.302 | 0.211 | 1.625 | 28 | | 0 | | 0 | |
| 14 | 0.0045 | 4.3 | 2.8 | 0.8 | 0.13 | 0.20 | 0.04 | 0.256 | 0.120 | 1.312 | 28 | | 0 | | 0 | |
| 15 | 0.0038 | 3.4 | 3.1 | 0.8 | 0.14 | 0.15 | 0.03 | 0.163 | 0.181 | 0.822 | 28 | | 0 | | 0 | |
| 16 | 0.0034 | 4.4 | 4.4 | 3.8 | 0.23 | 0.19 | 0.04 | 0.144 | 0.017 | 0.711 | 28.1894 | 0.0856 | 0.0727 | 0.1053 | 0.1012 | 0.117 |
| 17 | 0.0035 | 2.4 | 2.5 | 1.9 | 0.12 | 0.12 | 0.03 | 0.136 | 0.164 | 0.675 | 28.1936 | 0.0429 | 0.091 | 0.0627 | 0.127 | 0.064 |
| 18 | 0.0035 | 2.4 | 2.4 | 1.8 | 0.12 | 0.12 | 0.05 | 0.184 | 0.161 | 0.673 | 28.2089 | 0.0404 | 0.0726 | 0.0611 | 0.1175 | 0.0603 |

1. 3 Frames (2,3,4), Fixed XYZ Control Points.
2. 2 Frames (2,3).
3. Estimate interior orientation (IO), f,xp,yp.
4. Update exterior orientation (EO) using results from run 2. Do not estimate IO.
5. Assign statistical weights to EO parameters: XYZ = 10.0 m; omega, phi, kappa = 0.5 dec.degrees.
6. Estimate IO.
7. Assign GCP statistical weights, XYZ = 0.40 m.
8. IO NOT estimated.
9. Assign GCP statistical weights, XYZ = 0.20 m.
10. Update EO using results from run 9. Set EO statistical weights: XYZ = 7.0 m; omega,phi, kappa = 0.5 dec.degrees.
11. Estimate IO.
12. Add Frame 4. Update EO using results from run 11. Set EO (Frame 2, 3) statistical weights: XYZ = 4.0 m; omega, phi, kappa = 0.2 dec.degrees.
Set EO (Frame 4) statistical weights: XYZ = 25.0 m; omega, phi, kappa = 5.0 dec.degrees.
13. IO NOT estimated.
14. Remove tie points, 5,6,18 due to large XYZ point residuals.
15. Update Frame 4 EO using results from run 14. Set Frame 4 EO statistical weights: XYZ = 10.0 m; omega, phi, kappa = 0.5 dec.degrees.
16. Estimate IO.
17. Update EO using results from run 16. Set EO (Frame 2, 3, 4) statistical weights: XYZ = 4.0 m; omega, phi, kappa = 0.2 dec.degrees.
18. Estimate 4 additional parameters (AP).

Table 1. SCBA Results

inadequate stochastic model to reflect the quality of the exterior orientation initial approximations decreased the quality of results in Run 7. By excluding the interior orientation from the solution, greater precisions were attained. Continuing to strengthen the geometric quality of the input observations, GCP standard deviation assignments were decreased to 0.20 meters (Run 9). The resulting exterior orientation parameters determined from Run 9 were used to update the initial approximations. Corresponding standard deviation values of the newly estimated exterior orientation parameters were used as a guide in assigning statistical weights to the individual parameters (Run 10). The solution simultaneously decreased exterior orientation standard deviation values and GCP accuracies, thus indicating increased stability within the geometric network of photogrammetric observations and parameters. Due to the increased stability in defining the camera positions, the interior orientation parameters were estimated (Run 11). Low standard deviation values were maintained for the exterior orientation parameters although larger errors were computed for the X and Y GCP accuracies. The principal point offset in the x direction was lower than the corresponding standard error estimate, indicating minimal confidence in the recovery of the parameter. This can be attributed to large correlations existing between the exterior orientation and interior orientation and the sample and distribution of control and tie points within the two frames of imagery.

Based upon the results from Run 11, the initial approximations to the exterior orientation parameters were updated and new statistical weights were assigned to further constrain the observations. In order to increase the redundancy of data (imagery, control and tie points), frame 4 was introduced into the solution (Run 12). This resulted in increasing the exterior orientation standard deviation values, while maintaining the GCP accuracies. This can be attributed to relatively larger standard deviation assignments to the exterior orientation parameters of frame 4. This also negatively impacted the precise recovery of the interior orientation parameters. For example, the computed standard error for the principal point offset in the x and y direction was larger than the parameters themselves.

In order to stabilize the exposure station position and attitude for each frame, the interior orientation parameters were excluded from processing (Run 13). Due to relatively large tie point XYZ residuals, several points (t5, t6, and t18) were removed from the solution (Run 14). This positively impacted the overall solution by decreasing the exterior orientation standard deviation estimates while also increasing the accuracy of the GCPs. Based upon the results from Run 14, the initial exterior orientation approximations were updated along with their corresponding statistical weights (Run 15). The interior orientation parameters were then estimated (Run 16). The computed standard error for the principal point offset in the x and y direction remained larger than the parameters themselves. By decreasing the exterior orientation statistical weight assignments for each frame, this problem was resolved (Run 17). Continuing to constrain the functional model using the stochastic model decreased the standard deviation values for the exterior orientation parameters while also increasing the accuracy of the GCPs.

In order to compensate for radial lens distortion, differential image axis scaling and non-orthogonality between the x and y image axis, additional parameters were recovered (Run 18). Low standard deviation values were maintained for the exterior orientation parameters while also maintaining high GCP accuracies. Lower focal length and principal point offset

standard errors were achieved. Table 2 depicts four additional parameters, their associated standard errors and maximum impact in the x and y image direction.

| AP | Value (mm) | Standard Error | Max x (mm) | Max y (mm) |
|----|------------|----------------|------------|------------|
| 1 | -5.3 e-05 | 1.6 e-05 | -0.0111 | -0.0092 |
| 2 | 5.6 e-04 | 4.1 e-04 | 0.0031 | -0.0026 |
| 3 | 1.2 e-03 | 7.1 e-04 | 0.0055 | 0.0066 |
| 4 | -4.5 e-04 | 3.6 e-04 | 0.0000 | -0.0137 |

Table 2. Additional parameters and estimated precision's estimated using the SCBA

Additional parameter 1 accounts for radial lens distortion. Parameters 2 and 3 compensate for the non-orthogonality of the x and y image axis, while parameter 4 accounts for the differential scale in x and y pixel size. Table 3 depicts the image residuals for each frame.

| Frame | Points | x (mm) | Y (mm) |
|-------|--------|--------|--------|
| 2 | 18 | 0.0035 | 0.0046 |
| 3 | 20 | 0.0033 | 0.0062 |
| 4 | 11 | 0.0035 | 0.0061 |

Table 3. Image Residuals from the SCBA

The image residuals in the x direction are approximately 1/3 the image pixel size. The image residuals in the y direction are approximately 1/2 the image pixel size. The systematic difference between the x and y image residuals can be attributed to the differential scale factor in image pixel size.

7.1 Validation of Self-Calibrating Bundle Adjustment

Using the estimates for interior and exterior orientation, IMAGINE OrthoMAX was used to triangulate the strip of imagery, generate stereo pairs and DEMs. The exterior orientation parameters determined using IMAGINE OrthoBASE were imported and fixed in position. Stereo pairs were subsequently generated for later use in stereo editing. Using the three frames of imagery, two digital elevation models were automatically generated having a 1.0 meter resolution in the X and Y direction. Each DEM was edited using the point and polygon stereo-editing tools of IMAGINE OrthoMAX. The adjacent two DEMs were subsequently stitched using the ERDAS IMAGINE mosaic capabilities. Approximately 136,000 elevation postings were automatically collected for the area of interest within a time frame of 30 minutes.

The XYZ check point data was differenced from the full coverage DEM. The absolute mean difference in elevation was 0.586 meters. The standard deviation of the mean was 0.526 meters.

8. CONCLUDING REMARKS

The presented paper successfully extended the application of digital photogrammetry to landform modeling using a digital camera as a non-conventional image capture device. The accurate DEM results indicate that IMAGINE OrthoBASE and the techniques employed for self-calibration and bundle adjustment work very well with imagery collected using a digital camera. Minimal information was required with respect to providing initial approximations to the unknown exterior orientation parameters. A critical component of successfully utilizing the SCBA included the ability to incorporate a

stochastic model for the assignment of statistical weights to the input observations and unknown parameters. In using this approach, geometrically stable estimates to the exterior orientation parameters were established. Once these had been precisely estimated, interior orientation parameters were successfully recovered. This approach eliminated the negative impacts caused by the large correlations existing between the interior and exterior orientation parameters. The functional model used to recover the additional parameters had proven effective in estimating radial lens distortion, principal point offset, non-orthogonality of the x and y image axis and the scale differential in the image pixel size. It is safe to say that the use of digital cameras for close-range photogrammetry can be extended to aerial photogrammetric applications, preserving accuracy and overall quality equivalent to results which could be generated using metric cameras as the photographic data capture device.

Acknowledgements

This work was carried out within MEDALUS III Project IV, funded by EU contract ENV4-CT95-0118. The air survey was carried out by GeoTechnologies, a member of the Bath Spa University College Enterprises Limited group of companies, and we wish to thank Alex Koh and Dr. Rick Curr for their help in this campaign. We also thank Dr Jim Chandler and Mike Gooch, Loughborough University, for their assistance and the use of stereo editing equipment.

REFERENCES

- Chandler, J.H., and R. Moore, 1989. Analytical Photogrammetry: A Method for Monitoring Slope Instability. *Quarterly Journal of Engineering Geology*. Vol. 22, pp. 97-110.
- Chandler, J.H., and D. Brunsden, 1995. Steady state behaviour of the Black Ven mudslide: The application of archival analytical photogrammetry to studies of landform change. *Earth Surface Processes and Landforms*. Vol. 20, pp. 255-275.
- Collin, R.L., and N.W.T. Chisholm, 1991. Geomorphological Photogrammetry. *Photogrammetric Record*. Vol. 13, No. 78, pp. 845-854.
- Dixon, L.F.J., R. Barker, M. Bray, P. Farres, J. Hooke, R. Inkpen, A. Merel, D. Payne, A. Shelford, 1998. Analytical photogrammetry for geomorphological research. In: *Landform measurement, modelling and analysis*. John Wiley and Sons, Cambridge, pp. 466.
- Fraser, C.S., 1997. Digital camera self-calibration. *ISPRS Journal of Photogrammetry and Remote Sensing*, Vol. 52, pp. 149-159.
- Fryer, J.G., J.H. Chandler, and M.A.R. Cooper, 1994. On the accuracy of heighting from maps and aerial photographs: implications for process modellers. *Earth Surface Processes and Landforms*. Vol. 19, pp. 577-583.
- Kenefick, J.F., M.S. Gyer, and B.F. Harp, 1972. Analytical self-calibration. *Photogrammetric Engineering and Remote Sensing*. Vol. 38 pp. 1117-1126.
- Lane, S., K.S. Richards, and J.H. Chandler, 1993. Developments in photogrammetry; the geomorphological potential. *Progress in Physical Geography*. Vol. 17, No. 3, pp. 306-328.
- Lane, S. N., J. H. Chandler and K. S. Richards, 1994. Developments in monitoring and modelling small-scale river bed topography. *Earth Surface Processes and Landforms*, Vol. 19, pp. 349-368
- Smith, M., 1987. Photogrammetric techniques for archaeological mapping using oblique non-metric photography. Unpublished PhD thesis, University College London, 230pp.
- Stojic, M., J. H. Chandler, P. E. Ashmore and J. Luce, 1998. The assessment of sediment transport rates by automated digital photogrammetry. *Photogrammetric Engineering and Remote Sensing*, (In Press).
- Welch, R., and T.R. Jordan, 1983. Analytical non-metric close-range photogrammetry for monitoring stream channel erosion. *Photogrammetric Engineering and Remote Sensing*. Vol. 49, No. 3, pp. 367-374.